CCC Annual Report

UIUC, August 19, 2015

Investigation of Flow Pattern, Surface Behavior, and Mold Slag Entrainment using an Oil-Water Model and CFD Model

UIUC: Seong-Mook Cho, Brian G. Thomas

POSTECH: Seon-Hyo Kim, Hyoung-Jun Lee

Department of Mechanical Science & Engineering

University of Illinois at Urbana-Champaign

Research Background: Slag Entrainment Mechanisms

1. **Surface level fluctuation**[2-4]
2. Meniscus freezing, hook formation
3. **Vortex Formation**[5,6]
4. **Shear layer instability**[7-9]
5. **Upward flow**[10]
6. Argon bubble interactions/slag foaming
7. **Slag crawling**[11]
8. **Surface wave instability**
9. **Surface balding**

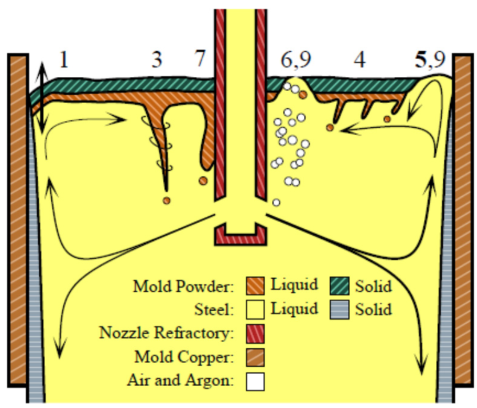

<Slag Entrainment Mechanisms[1]>

- Primary mechanism of slag entrainment depends on casting conditions, but likely involve mechanisms **1,8 (mainly surface)** and **3, 4, 5, 7, 9 (mainly interior)** which all have both quasi-steady and transient aspects.
- Investigate surface flow and entrainment phenomena using **water model experiments, plant measurements and advanced computational models to quantify slag entrainment in a continuous slab casting**
- **Computational model is available to evaluate slag entrainment criteria**

Research Scope

- **Objectives:**
  - Understand flow patterns, surface behavior, related to slag entrainment in mold of continuous slab caster.
  - Develop computational models of “liquid slag/molten steel interface motion and slag entrainment at mold surface”.
  - Apply the validated computational model with water model experiments, to get insight into slag entrainment mechanism in mold of continuous slab casting.

- **Methodologies:**
  - **1/3 scale water model experiments** to understand mold flow pattern and evaluate slag entrainment mechanisms.
  - **Computational modeling** to evaluate 3D-Volume Of Fluid (VOF) model to predict mold flow pattern for 1/3 scale water model of conventional slab caster with clog nozzle and validate the model prediction with **water model experiments**.

Review of 1/3 Scale Water Model Measurements

1/3 Scale Water Model

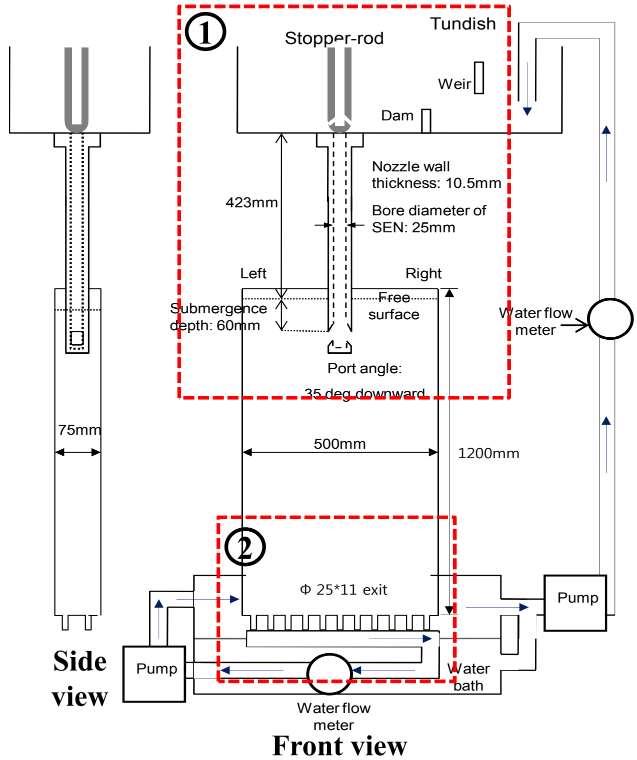

<Schematic>

<Photos>

Caster Dimensions and Process Conditions

Caster dimensions		
	1/3 scale water model	Real caster (normal case)
Nozzle bore diameter (inner/outer)	25 mm/46 mm	75 mm/138 mm
Nozzle bottom well depth	6.3 mm	19 mm
Nozzle port area	non-clogged port: 23.3 mm x 26.7 mm clogged port: 13.5 mm x 15.4 mm	69.9 mm x 80.1 mm
Nozzle port angle	35 down degree at both top and bottom	35 down degree at both top and bottom
Mold thickness	77 mm	231 mm
Mold width	500 mm	1500 mm
Process conditions		
Volume flow rate (Water or Steel)	34.4 LPM	536.2 LPM (3.76 T/min)
Casting speed	$u_{c,W}$: 0.89 m/min	$u_{c,R}$: 1.54 m/min
Submerged depth of nozzle	60 mm	180 mm

- Flow similarity between 1/3 scale water model (Case W) and real caster (Case R)

➡ Froude number (ratio of inertia force to gravitational force): $\left(u/\sqrt{gL}\right)_W = \left(u/\sqrt{gL}\right)_R$

Casting speed $u_{c,W}$ for 1/3 scale water model: $u_{c,W} = u_{c,R}\sqrt{L_W/L_R}$

Details of Nozzle Dimensions

No-clog nozzle	Clog nozzle

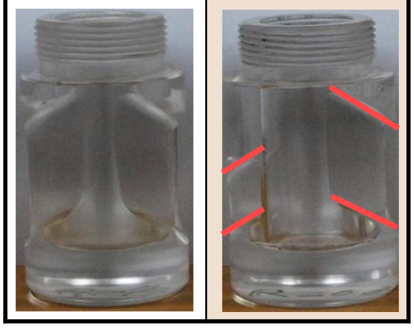

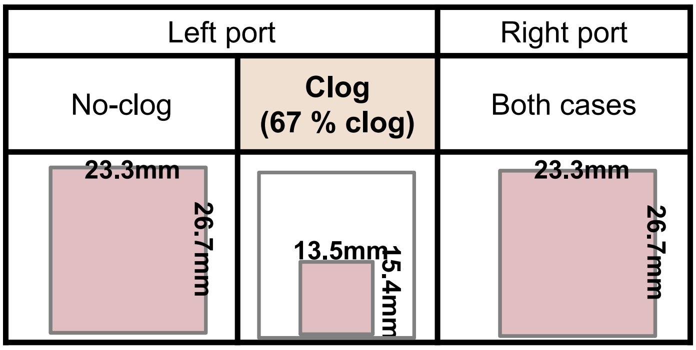

Dimension of nozzle port		No-clog	Clog
Right	Width (mm)	23.3	23.3
	Height (mm)	26.7	26.7
Left	Width (mm)	23.3	13.5
	Height (mm)	26.7	15.4
Ratio of area between left and right		*1*	*0.33*
Ratio of area between two ports and nozzle bore		*2.54*	*1.69*
Port angle (degree)		-35	-35

- To investigate effect of asymmetric mold flow on surface behavior and mold slag entrainment, two cases (No-clog nozzle and Clog nozzle) are compared.
- Clog nozzle has 67%-clog part in upper region of left port.

Comparison of Properties between Oil/Water and Mold Flux/Steel System

	Water model		Real caster	
	Silicon oil	Water	Mold flux	Molten steel
Temperature	25°C		1200 ~ 1400°C	1600°C
Density	963.3 kg/m³	998.2 kg/m³	Bulk: 750 kg/m³, Liquid: ~3000 kg/m³	7020 kg/m³
Density ratio	0.965 (Oil/Water)		0.427 (Liquid mold flux/Molten steel)	
Dynamic viscosity	0.0963 kg/m·sec	0.0010 kg/m·sec	0.160 kg/m·sec (1400°C) 0.345 kg/m·sec (1300°C) 0.781 kg/m·sec (1200°C)	0.0067 kg/m·sec
Dynamic viscosity ratio	96.3 (Oil/Water)		23.9 (Mold flux at 1400°C/Molten steel)	
Kinematic viscosity	0.0001 m²/sec	1.002 x 10^{-6} m²/sec	0.533 x 10^{-4} m²/sec (1400°C) 1.150 x 10^{-4} m²/sec (1300°C) 2.603 x 10^{-4} m²/sec (1200°C)	0.954 x 10^{-6} m²/sec
Kinematic viscosity ratio	99.8 (Oil/Water)		55.9 (Mold flux at 1400°C/Molten steel)	
Surface tension	0.0209 N/m	0.0720 N/m	0.437 N/m	1.78 N/m
Interfacial tension	0.0247 N/m		1.34 N/m	

- Higher density ratio, lower dynamic viscosity of upper layer, and lower interfacial tension produce more slag entrainments in silicon oil/water system than slag/steel system
- It is needed to understand entrainment phenomena in oil/water system and develop computational model for slag/steel system of real caster

Mold Surface Behaviors in Oil/Water System

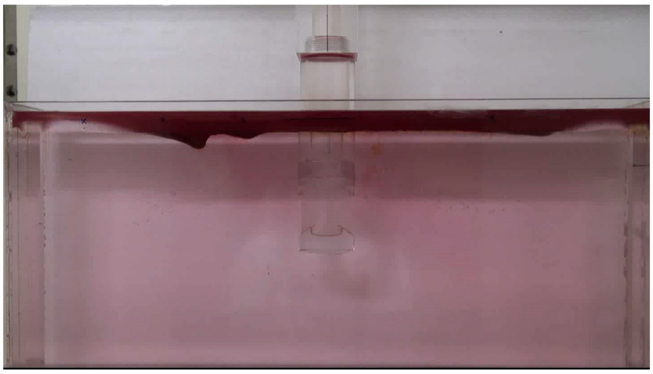

<No-clog case>

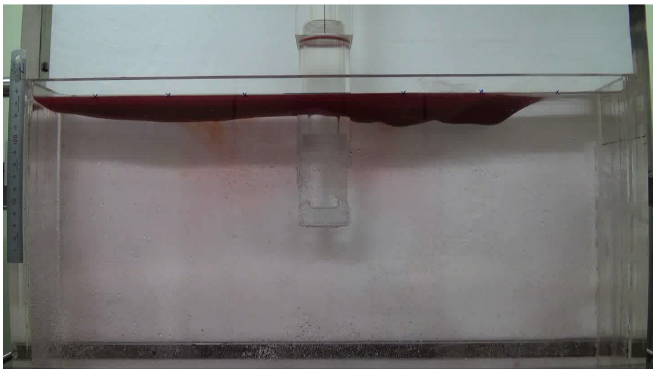

<Clog case>

- No-clog case shows surface level fluctuations, max ~ 20mm (~ 200 % of oil thickness average (10mm)). On the other hand, clog case produces much more severe surface instability over ~ 60 mm (~ 600 % of oil thickness average), which makes oil reach jet flow from nozzle port.
- **With clog nozzle,** surface instability is high enough to **drag oil** finger deep into nozzle port flow, resulting in oil **entrainment**.

Slag Entrainment Phenomena

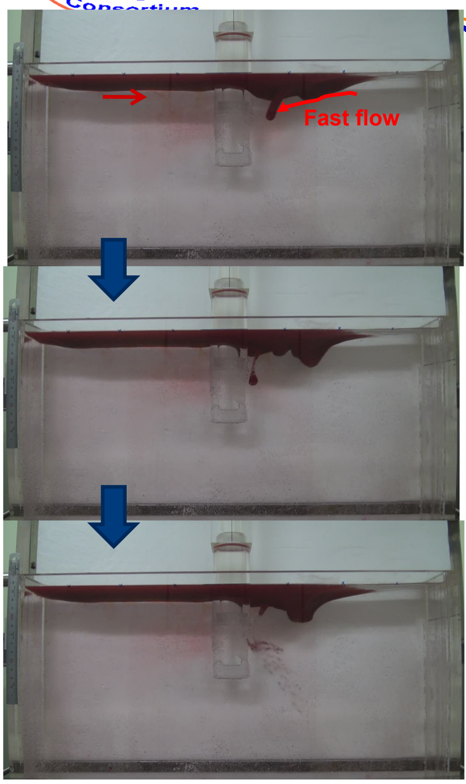

< Small entrainment >

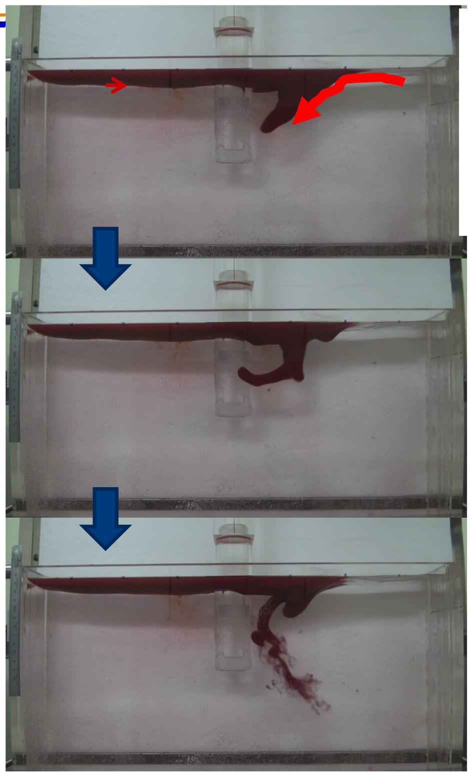

< Large entrainment >

- Abnormally fast surface flow induces interface instability between oil and water phase, dragging oil finger into water pool

- Entrained oil reaches nozzle port

- Entrained oil is "broken-up" into small sizes
- Jet flow takes oil bubbles deep into the mold

Critical Surface Velocity for Entrainment: Shear Layer Instability

- Shear layer instability mechanism is most likely to occur in the surface region where surface velocity shows a maximum
- Kelvin-Helmholtz (K-H) instability[7,8]:

$$\Delta V_{crit} = \sqrt[4]{4g(\rho_l - \rho_u)\Gamma_{ul}\left(\frac{1}{\rho_u}+\frac{1}{\rho_l}\right)^2}$$

- Funada-Joseph (F-J) instability[9]:

$$\Delta V_{crit} = \sqrt[4]{4g(\rho_l - \rho_u)\Gamma_{ul}\left\{\frac{(\mu_l+\mu_u)^4}{(\rho_u\mu_l^2+\rho_l\mu_u^2)^2}\right\}}$$

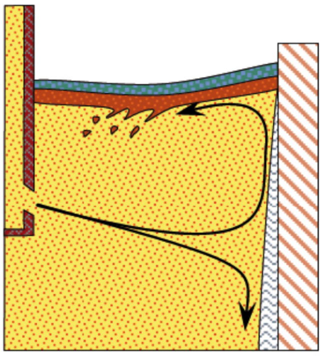

<Entrainment by shear layer instability[1]>

l: lower layer (water or molten steel)
u: upper layer (oil or molten slag)

ΔV_{crit}	Critical velocity difference between upper and lower layer (m/sec)
ρ	Density (kg/m^3)
Γ_{ul}	Interfacial tension between upper and lower layer (N/m)
μ	Dynamic viscosity (kg/m·sec)
g	Gravity acceleration (m/sec^2)

ΔV_{crit}	K-H	F-J
Oil/water	0.102 m/sec	0.072m/sec
Slag/steel	0.30 m/sec	0.27 m/sec

- With employing slag viscosity, F-J predicts smaller critical surface velocity

Critical Surface Velocity for Entrainment: Upward Flow

Harman and Cramb[10]:

$$V_{critical} = 3.065\frac{\Gamma_{ul}^{0.292}g^{0.115}}{\delta^{0.365}}\frac{(\rho_l-\rho_u)^{0.215}}{\rho_u^{0.694}}\frac{\mu_u^{0.231}}{\mu_l^{0.043}}$$

(a)

(b)

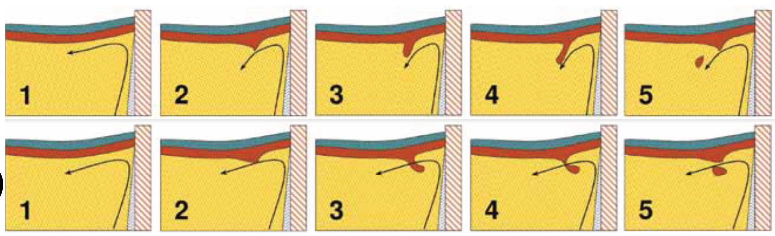

<Entrainment by upward flow with (a) dragging mode, (b) cutting mode[1]>

$V_{critical}$	**Critical surface velocity (m/sec)**
ρ	**Density (kg/m^3)**
μ	**Dynamic viscosity (kg/m·sec)**
Γ	**Interfacial tension between upper and lower layer (N/m)**
δ	**Upper layer thickness (m)**
g	**Gravity acceleration (m/sec^2)**

	$V_{critical}$
Oil/water (m/sec)	**Critical: 0.10 m/sec**
Slag/steel (m/sec)	**Critical: 0.44 m/sec**

Comparison of Critical Velocity for Entrainment between Predictions and Measurement (1/3 Scale Water Model)

Eddy-current sensor measurement of critical velocity for entrainment:

Critical velocity (water model with no-oil) which includes 17 # abnormal sudden surface velocity increase.

(Entrainment occur 3 times during 180 sec → 17# /1000sec)

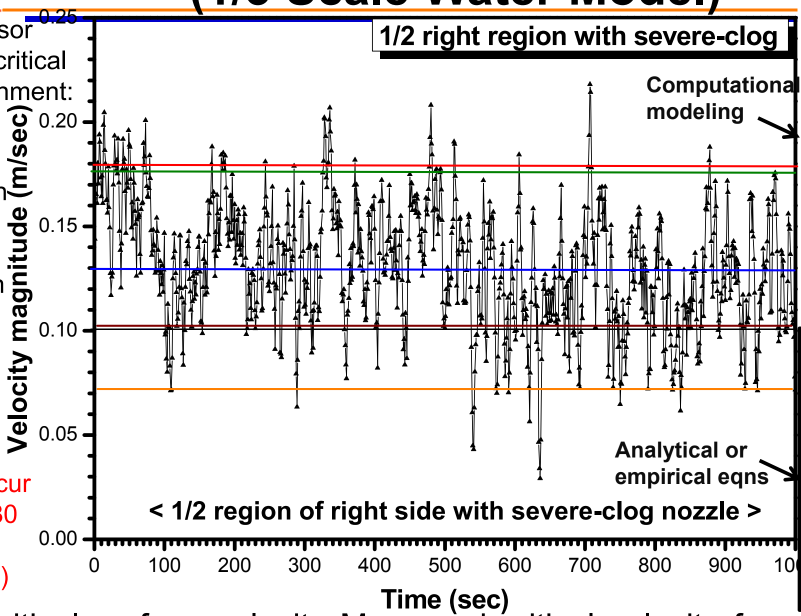

~0.180 m/sec: measured critical velocity magnitude for entrainment

~0.18 m/sec: predicted critical velocity by Cho's simulation

0.175 m/sec: Predicted critical velocity magnitude by Hibbeler's simulation[4]

0.130 m/sec: mean velocity magnitude

0.102 m/sec: Kevin-Helmholtz
0.072 m/sec: Funada and Joseph
Predicted critical velocity magnitude for shear instability

0.10 m/sec: predicted critical velocity magnitude for upward flow (Harman and Cramb)

- Predicted critical surface velocity Measured critical velocity for entrainment is higher than predicted ones by the reported eqns for shear instability (K-H, F-J) and upward flow (H-C).
- Cho's and Hibbeler's simulation results well-match with the measured one, indicating excellent potential computational modeling for future work.
- Computational modeling work is needed to understand slag entrainment mechanism in

3D-VOF Model Test: LES coupled VOF Modeling of Surface Motion and Entrainment Phenomena

(Modeling of Oil/Water System in 1/3 scale water model)

Governing Equations

Large Eddy Simulation (LES) coupled with Volume Of Fluid (VOF) for three-phase (air/oil/water) flows

- **VOF** (Volume fraction of each phase):

$$\frac{\partial \alpha_{air}}{\partial t} + \nabla \cdot \left(\alpha_{air} \cdot \overrightarrow{u_{air}}\right) = 0$$

air volume fraction

$$\frac{\partial \alpha_{oil}}{\partial t} + \nabla \cdot \left(\alpha_{oil} \cdot \overrightarrow{u_{oil}}\right) = 0$$

oil volume fraction

$$\alpha_{water} = 1 - \alpha_{oil} - \alpha_{air}$$

water volume fraction

- **Continuity:**

$$\frac{\partial \rho_{mix}}{\partial t} + \nabla \cdot \left(\rho_{mix}\vec{u}\right) = 0 \qquad \rho_{mix} = \alpha_{water}\rho_{water} + \alpha_{oil}\rho_{oil} + \alpha_{air}\rho_{air}$$

- **Momentum conservation:**

$$\rho_{mix}\frac{\partial u}{\partial t} + \rho_{mix} u \cdot \nabla u = -\nabla p + \nabla \cdot \left[\mu_{mix}\left(\nabla u + \nabla^T u\right)\right] + \rho_{mix} g + F_{interface}$$

Domain and Mesh

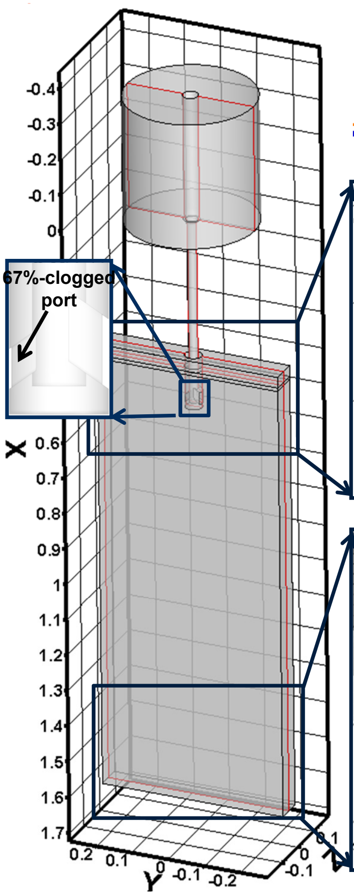

<Domain>

Hexahedral cells: ~2.8 million

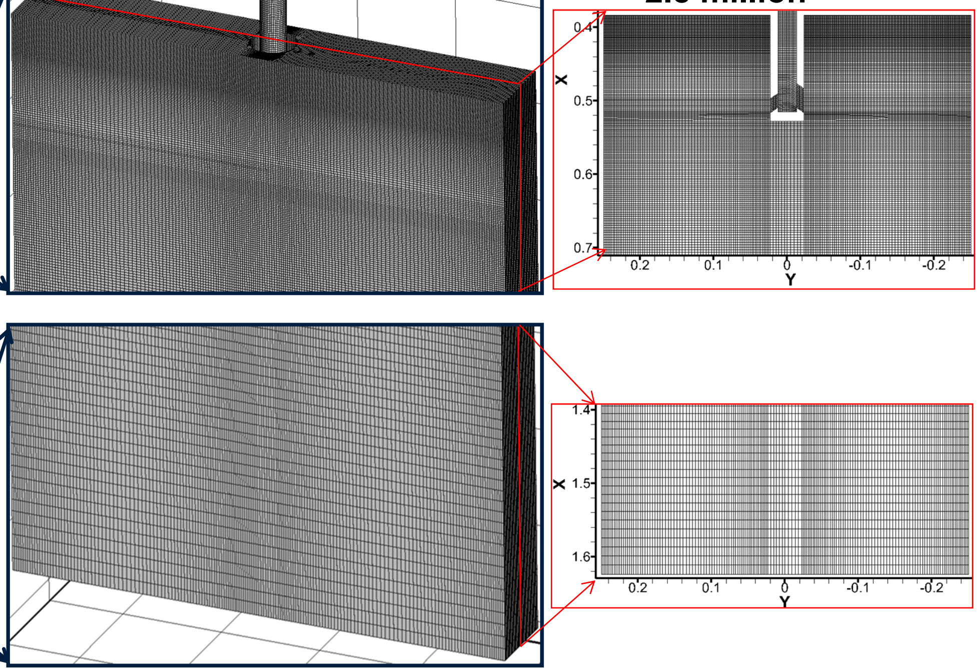

<Mesh>

Boundary Conditions and Computation Details

- Boundary conditions:

Inlet (tundish)	0.00149 m/s
Air/Oil interface and Oil/Water interface	interior
Top surface of air layer	0 shear stress
Stopper-rod walls, Nozzle walls, wide faces, and narrow faces	No slip

- Contact angle[12-14]
  - air/water/acrylic: 69.1°
  - Air/oil/acrylic: 26.6°
  - Oil/water/acrylic: 76.1°
- Interfacial tension
  - Oil / water interfacial tension: 0.247 N/m
  - Air / oil interfacial tension: 0.209 N/m
- Initial input values:
  - Velocity field of steady-state single-phase (water) flow using standard k-ε CFD model
  - 100% air fraction in initial air layer, 100% oil fraction in initial oil layer, 100% water fraction in initial water pool
- Time step: 0.001 sec

Initial Input Values for VOF Model

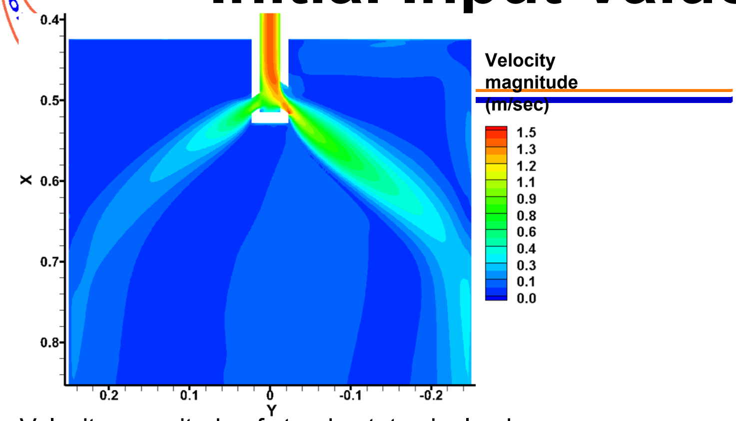

<Velocity magnitude of steady-state single phase (water) flow from standard k-ε model>

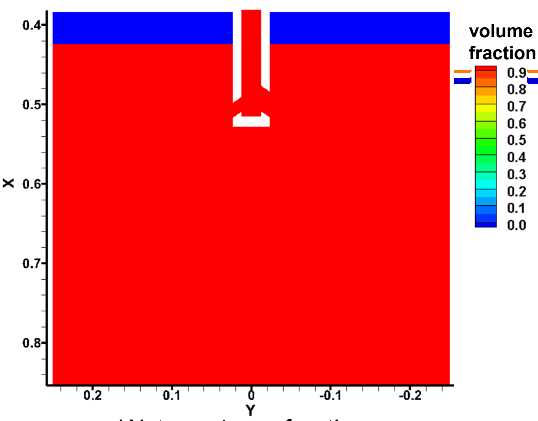

<Water volume fraction>

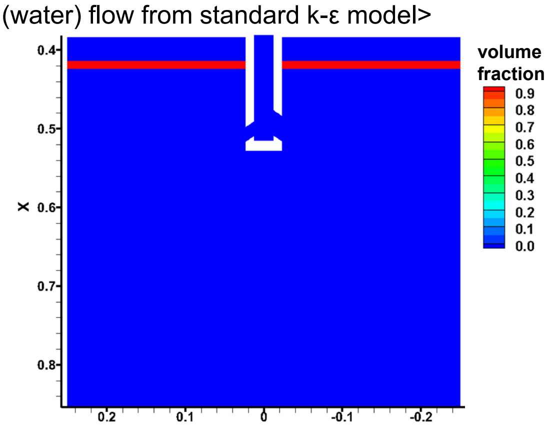

<Oil volume fraction>

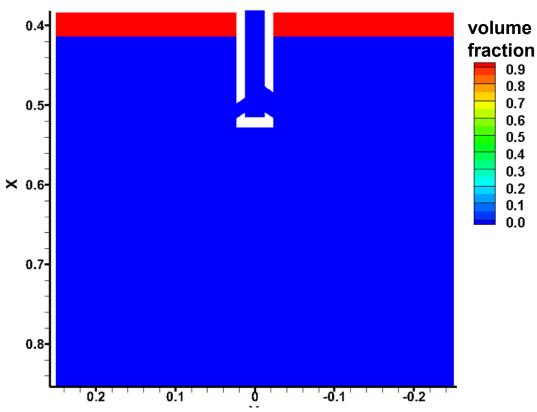

<Air volume fraction>

Planes and Points in the Domain

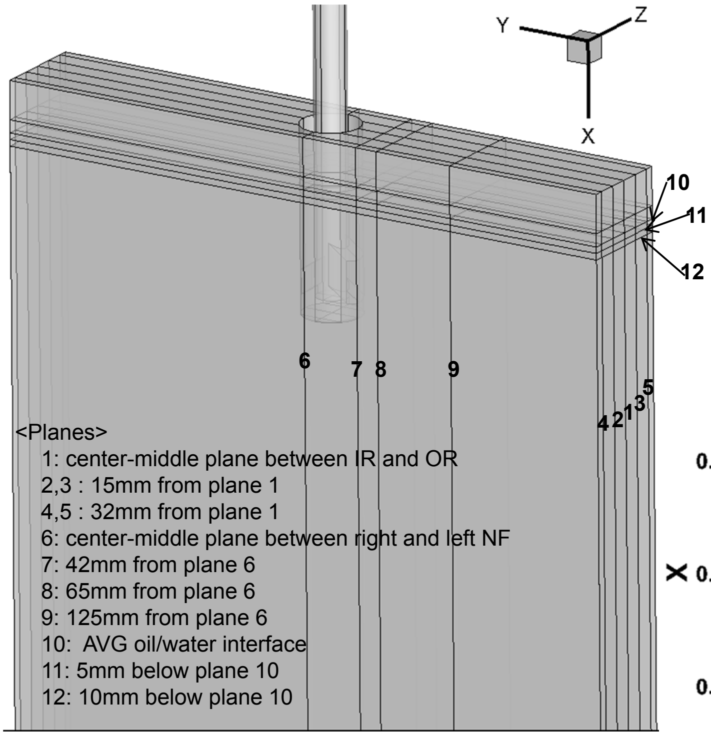

<Planes in the mold domain>

Plane data: collected at 0.05 s interval
Point data: collected at 0.001s interval

77 mm (mold thickness) X 500 mm (mold with)

<Points>
P1 (512, -23, 0)
P2 (512, 23, 0)
P3 (600, -125, 0)
P4 (600, 125, 0)
P5 (433.8, -125, 0)
P6 (433.8, 125, 0)

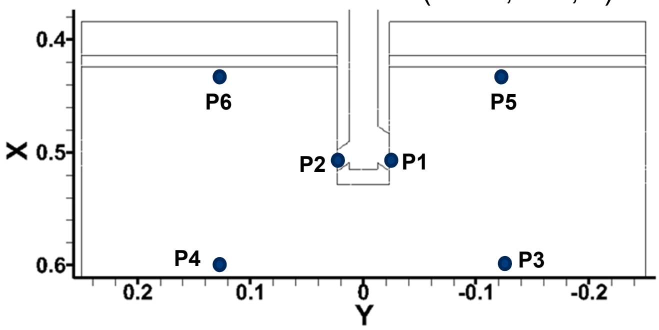

<Points in the mold domain>

Flow Pattern in Clog Nozzle and Mold

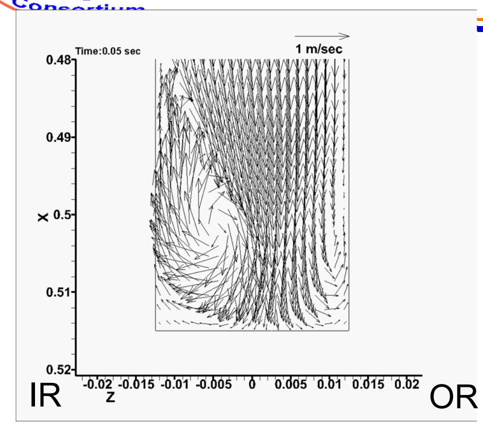

<Nozzle swirl at bottom region>

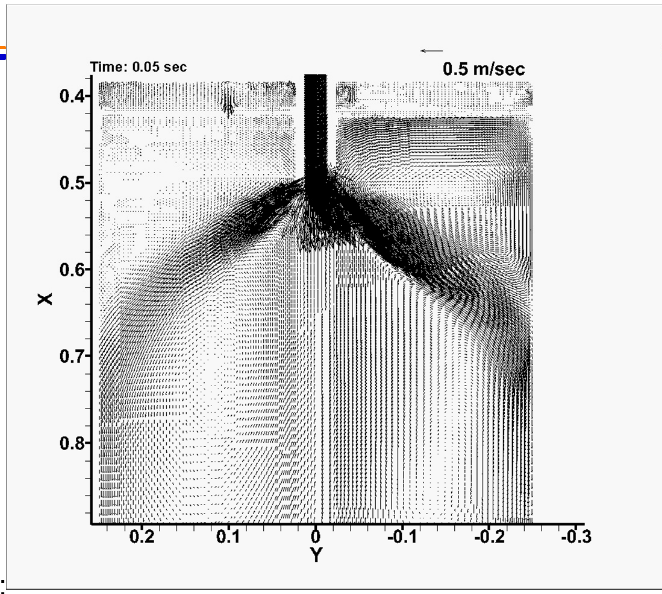

<Asymmetric mold flow pattern at Plane 1>

- **Nozzle swirl** shows **clockwise** or **counter-clockwise** directions with ~3sec time intervals: direction change phenomena well-matches with the measurement[15]
- **Asymmetric flow pattern** is induced **between left/right NF** and **between IR/OR** in the mold, by nozzle clogging (unbalanced double-roll pattern).
- **With clogged nozzle, surface flow from right side** cross the surface and **suppress the uprising flow from left NF**

Jet Velocity Histories in the Nozzle and Mold

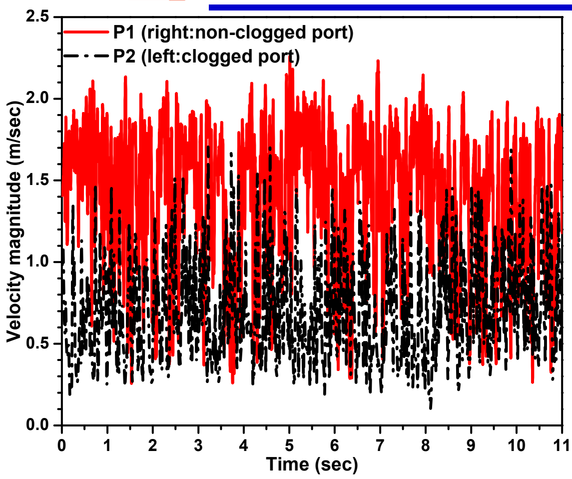

<Nozzle port >

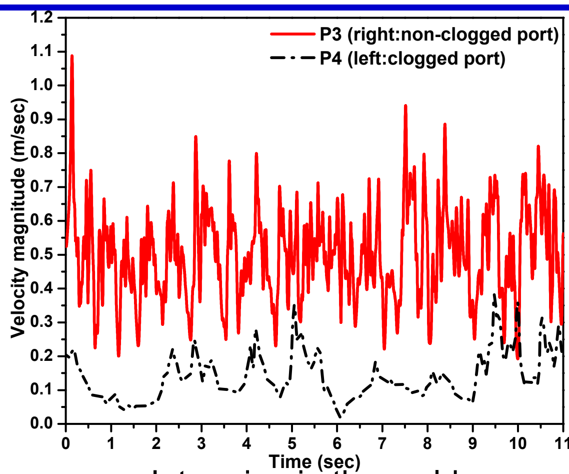

<Jet region in the mold>

	Average (m/sec)	Standard deviation (m/sec)
P1	1.41	0.42 : 29.8 % of Avg
P2	0.71	0.30: 42.3 % of Avg
P3	0.50	0.13: 26.0 % of Avg
P4	0.14	0.07: 50.0% of Avg

- Faster jet flow with more velocity fluctuations from non-clogged nozzle port.
- High-frequency high-amplitude jet flow from non-clogged port and low-frequency low-amplitude from clogged port.

Surface Flow Patterns with Clog Nozzle

Plane heights in slide 19

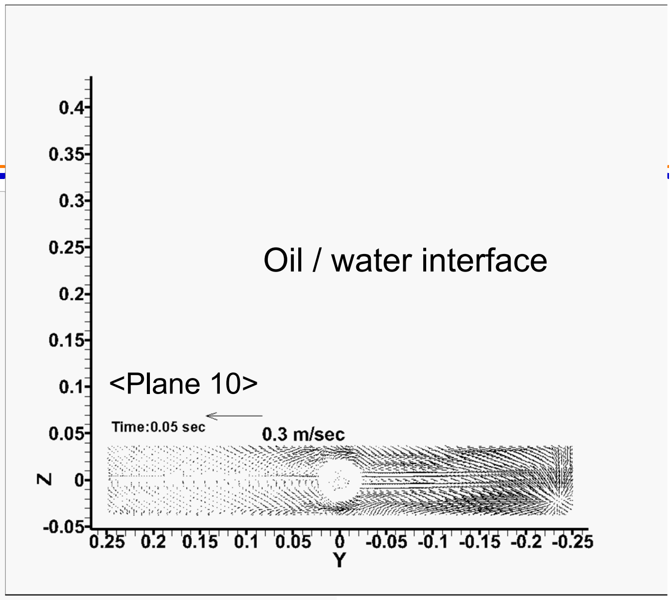

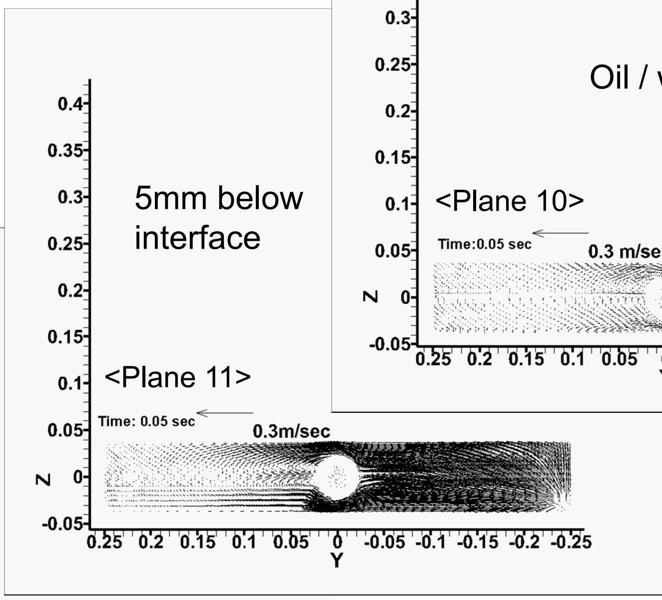

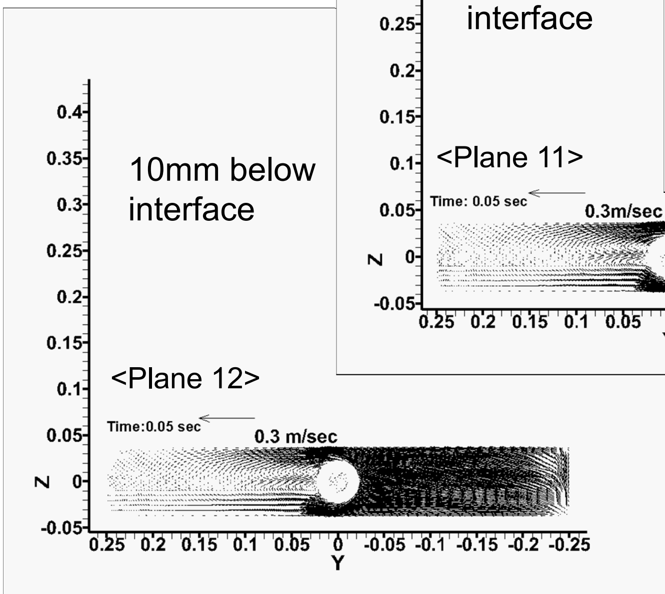

- With a clogged left port, the stronger surface flow from the right side overcomes flow from the left side.
- Vortices near SEN, starting at interface

Oil Volume Fraction at Plane 1,4,5

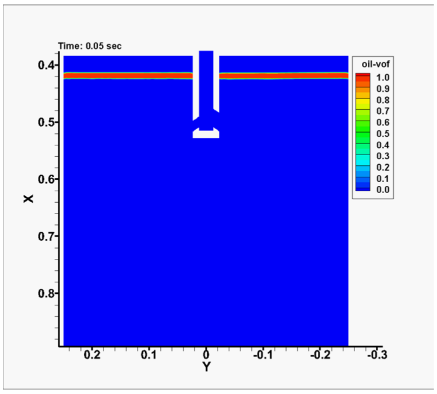

<Plane 1:center-middle plane>

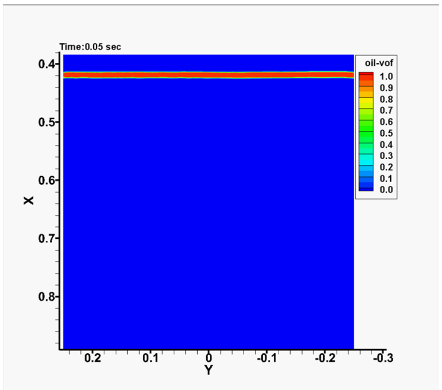

<Plane 4: 7mm from IR>

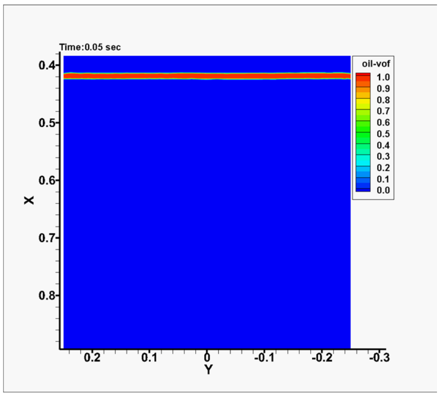

<Plane 5: 7mm from OR>

- Oil layer at right side (non-clogged nozzle port side) becomes thinner with higher surface flow
- Oil layer on center-middle plane is thinner than other regions (near IR, OR) due higher surface velocity

Oil Volume Fraction at Plane 6-8

Endview
(centerplane)

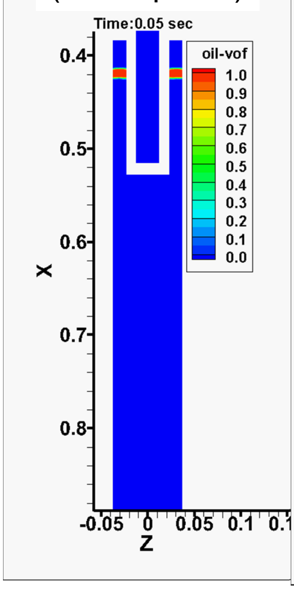

<Plane 6>

Endview
(42 from SEN)

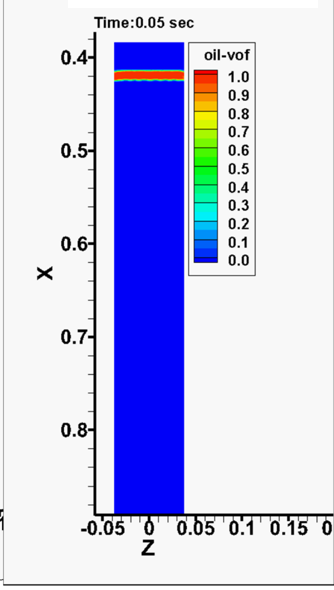

<Plane 7>

Endview from NF
(65 from center of SEN)

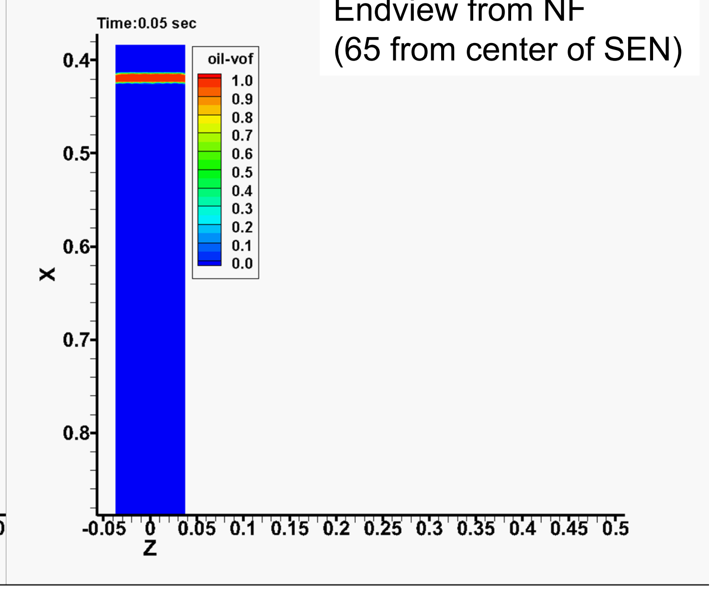

<Plane 8>

- Transient asymmetric surface flow between IR and OR produces non-uniform oil layer thickness
- Oil layer thickness decreases towards NF, especially in center region between IR and OR

Oil Volume Fraction at Plane 10-12

Plane heights
in slide 19

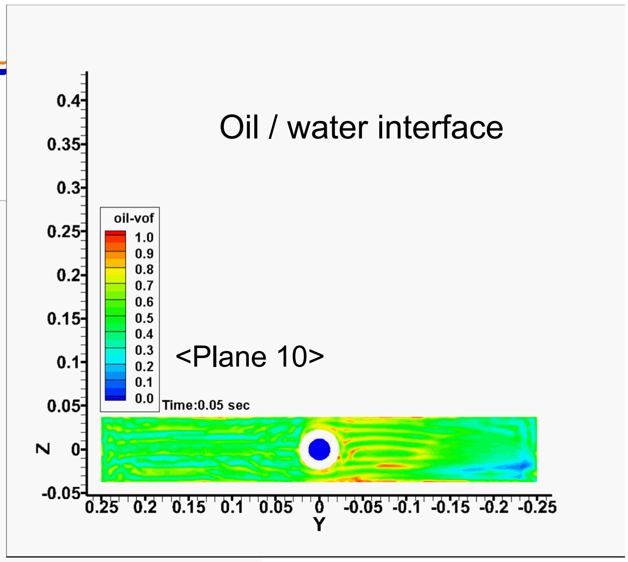

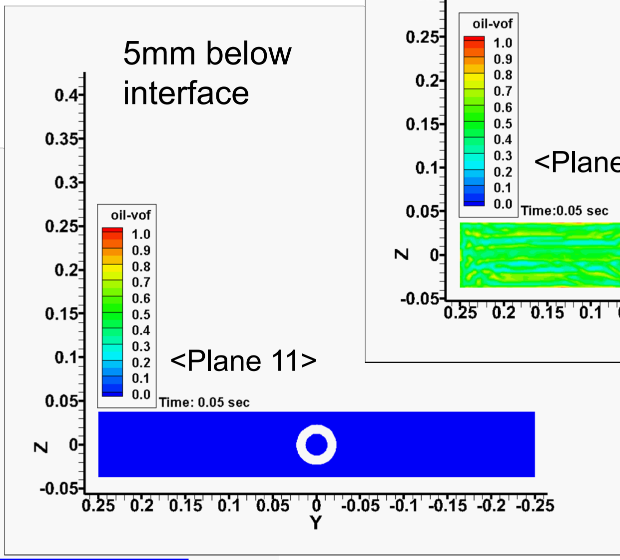

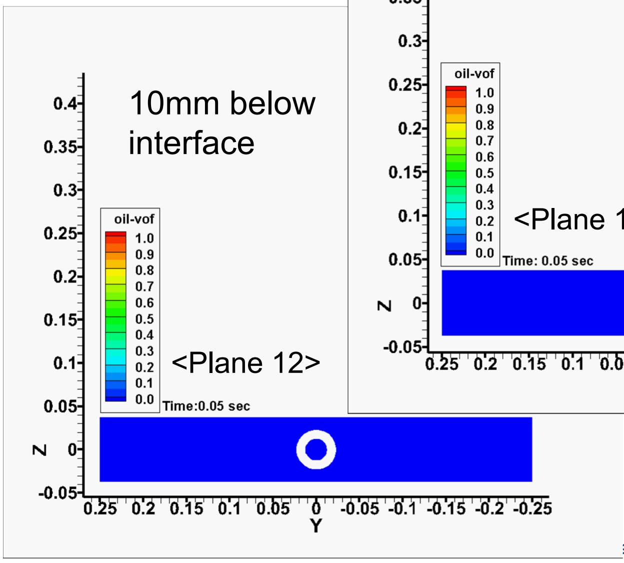

- Higher surface flow from right side seems to drags oil layer (from the interface between oil and water) into water pool.

Surface Velocity Histories and Oil Entrainment

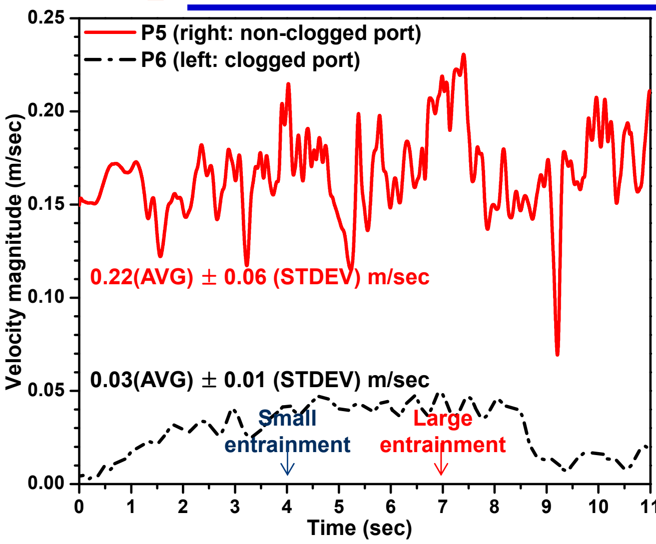

<Surface Velocity Histories and entrainment events>

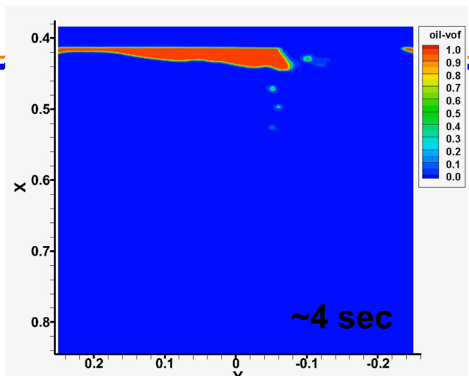

<**Small entrainment** at Plane 4 >

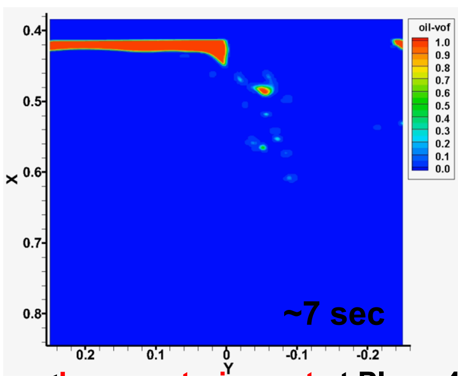

<**Large entrainment** at Plane 4 >

- **Entrainment** is induced by **momentum accumulation (dependent on critical surface velocity and its duration)** on oil layer.
- Thus, large entrainment follows after small entrainment. This trend is revealed from both the experiment and the LES coupled with VOF

3D-View of Oil Entrainment Phenomena by Time

3D iso-surface view of oil volume fraction 0.1 %

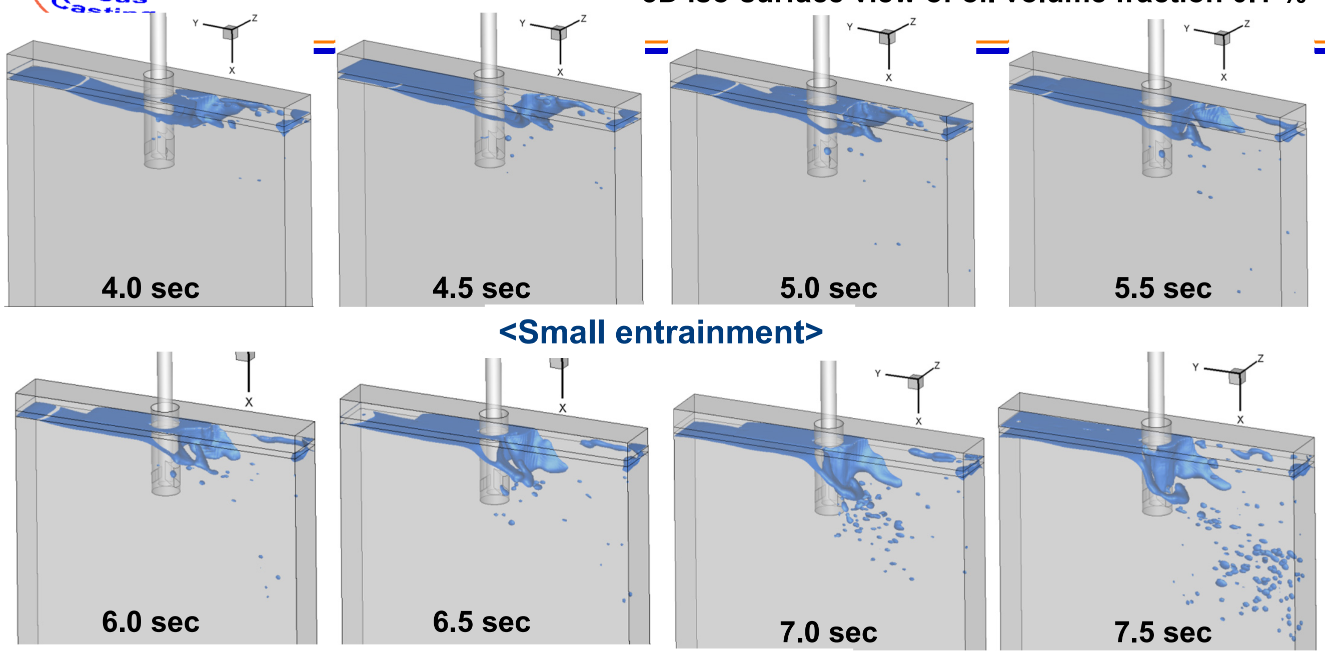

<Large entrainment>

- For ~4 and ~7 sec, oil entrainments occur with higher surface velocity over ~0.18* m/sec
- LES coupled with VOF model results (**oil/water interface motion, oil entrainment, critical surface velocity for entrainment**), show good agreements with those of water model experiments

Summary

- 3D-VOF LES model was applied to predict surface motion and entrainment in 1/3-scale oil/water model with clogged nozzle
- The model captures transient nozzle swirl and asymmetric mold flow between left/right NF and between IR/OR, by nozzle clogging.
- Transient asymmetric surface flows produce non-uniform oil layer thickness between left/right NF and IR/OR.
- Oil layer becomes thinner with higher surface flow.
- Abnormal fast surface flow towards SEN drags oil finger into water; then cuts off the entrained oil.
- Entrainment is induced by momentum accumulation (dependent on critical surface velocity and its duration) on oil layer: large entrainment follows after small entrainment. This trend is revealed from both the experiment and the LES coupled with VOF
- The predictions (oil/water interface motion, oil entrainment, critical surface velocity for entrainment), show good agreement with the water model experiments and indicate excellent potential of the LES model to predict slag/steel interface motion and slag entrainment in a mold of real caster.

Acknowledgments

- Continuous Casting Consortium Members (ABB, AK Steel, ArcelorMittal, Baosteel, JFE Steel Corp., Magnesita Refractories, Nippon Steel and Sumitomo Metal Corp., Nucor Steel, Postech/ Posco, SSAB, ANSYS/ Fluent)
- POSCO (Grant No. 4.0011721.01)
- Dae-Woo Yoon, POSTECH for help with the 1/3 scale water model experiments
- Ji-Joon Kim, Jong-Wan Kim, Yong-Hwan Kim, POSCO for discussion

References

1. L. C. Hibbeler, R. Liu, and B. G. Thomas: Proc of the 7th European Continuous Casting Conference, Steel Institute VDEh, 2011
2. T. Teshima, M. Osame, K. Okimoto and Y. Nimura: Poceedings of 71 Steelmaking Conference, pp. 111–118, The Iron and Steel Society, 1988
3. H. Nakamura, S. Kohira, J. Kubota, T. Kondo, M. Suzuki, and Y. Shiratani: Steelmaking Conference Proceedings, pp. 409-415, The Iron and Steel Society, 1992
4. J. Kubota, K. Okimoto, A. Shirayama, and H. Murakami: Steelmaking Conference Proceedings, pp. 233-241, The Iron and Steel Society, 1991
5. N. Kasai and M. Iguchi: ISIJ Int., 2007, Vol. 47, pp. 982-987
6. D. Gupta and A.K. Lahiri: Ironmaking and Steelmaking, 1996, Vol. 23, No. 4, pp. 361–363
7. H. L. F. Von Helmholtz: Monatsberichte der Koniglichen, 1868, Vol. 23, pp. 215-228
8. W. Thomson: Philosophical Magazine, 1871, Vol. 42, pp. 362-377
9. T. Funada and D. D. Joseph: J. Fluid, 2001, Vol. 445, pp. 263-283
10. J. M. Harman and A.W. Cramb: 79 Steelmaking Conference Proceedings, The Iron and Steel Society, 1996, pp. 773-784
11. J. Yoshida, T. Ohmi, and M. Iguchi: ISIJ Int., 2005, Vol. 45, pp.1160-1164
12. Surface tension between water and acryl: http://www.accudynetest.com/polytable_01.html
13. Mohammad Ilyas KHAN and Mohamed Mahmoud NASEF: Leonardo Journal of Sciences, 2009, Issue 14, pp. 18-30
14. Derrick O. Njobuenwu: AU J.T. 2007, Vol. 10(3), pp. 163-168
15. Hershey, D. E., B. G. Thomas, and F. M. Najjar: International Journal for Numerical Methods in Fluids, 17:1, 23-47, 1993.